2440–2450 *Nucleic Acids Research, 2007, Vol. 35, No. 7* *Published online 29 March 2007*
doi:10.1093/nar/gkm009

Structure of the intramolecular human telomeric G-quadruplex in potassium solution: a novel adenine triple formation

Jixun Dai[1], Chandanamali Punchihewa[1], Attila Ambrus[1], Ding Chen[1], Roger A. Jones[2] and Danzhou Yang[1,3,4,*]

[1]College of Pharmacy, The University of Arizona, 1703 E. Mabel St, Tucson, AZ 85721, USA, [2]Department of Chemistry and Chemical Biology, Rutgers University, 610 Taylor Road, Piscataway, NJ 08854, USA, [3]Arizona Cancer Center, 1515 N. Campbell Avenue, Tucson, AZ 85724, USA and [4]BIO5 Institute, The University of Arizona, 1140 E. South Campus Dr, Tucson, AZ 85721, USA

Received September 08, 2006; Revised December 21, 2006; Accepted December 27, 2006

ABSTRACT

We report the NMR solution structure of the intramolecular G-quadruplex formed in human telomeric DNA in K^+. The hybrid-type telomeric G-quadruplex consists of three G-tetrads linked with mixed parallel–antiparallel G-strands, with the bottom two G-tetrads having the same G-arrangement (*anti:anti:syn:anti*) and the top G-tetrad having the reversed G-arrangement (*syn:syn:anti:syn*). The three TTA loop segments adopt different conformations, with the first TTA assuming a double-chain-reversal loop conformation, and the second and third TTA assuming lateral loop conformations. The NMR structure is very well defined, including the three TTA loops and the two flanking sequences at 5′- and 3′-ends. Our study indicates that the three loop regions interact with the core G-tetrads in a specific way that defines and stabilizes the unique human telomeric G-quadruplex structure in K^+. Significantly, a novel adenine triple platform is formed with three naturally occurring adenine residues, A21, A3 and A9, capping the top tetrad of the hybrid-type telomeric G-quadruplex. This adenine triple is likely to play an important role in the formation of a stable human telomeric G-quadruplex structure in K^+. The unique human telomeric G-quadruplex structure formed in K^+ suggests that it can be specifically targeted for anticancer drug design.

INTRODUCTION

Telomeres are specialized DNA sequences that cap the ends of linear chromosomes. Human telomeric DNA consists of tandem repeats of the hexanucleotide $d(5'\text{-TTAGGG})_n$ for 5–8 kb in length toward the chromosome end, terminating in a single-stranded 3′-overhang of 100–200 bases in length (1–5). In normal cells, each cell replication results in a 50–200 base loss of the telomere, and after reaching a critical shortening of the telomeric DNA, the cell undergoes apoptosis or programmed cell death (6). In contrast, telomeres of cancer cells do not shorten on replication due to the activation of a reverse transcriptase telomerase that extends the telomeric sequence at the chromosome ends (7). Telomerase has been shown to be activated in 80–85% of human cancer cells (8), and has been suggested to play a key role in maintaining the malignant phenotype by stabilizing telomere length and integrity (9).

The structure and stability of telomeres are of great research interest as they are closely related with cancer (10–13), aging (14,15) and genetic stability (16–18). The G-rich telomeric sequence can fold into a G-quadruplex, a DNA secondary structure consisting of stacked G-tetrad planes connected by a network of Hoogsteen hydrogen bonds and stabilized by monovalent cations, such as Na^+ and K^+. Human telomeric DNA repeats are highly conserved, which has been suggested to be related to their ability to form DNA G-quadruplexes (13,19). The formation and stabilization of the DNA G-quadruplex in the human telomeric sequence have been shown to inhibit the activity of telomerase. Thus the telomeric DNA G-quadruplex has been considered to be an attractive target for cancer therapeutic intervention (10,12,13,20–22).

Structural information on the intact human telomeric DNA G-quadruplex formed under physiologically relevant conditions is necessary for structure-based rational drug design. We have very recently determined the folding structure of the intramolecular human telomeric G-quadruplex formed in K^+ solution by NMR, which

*To whom correspondence should be addressed. Tel: +1 520 626 5969; Fax: +1 520 626 6988; Email: yangd@pharmacy.arizona.edu

demonstrates a novel hybrid-type folding topology with mixed parallel–antiparallel G-strands (23). This hybrid-type G-quadruplex structure appears to be the physiologically relevant conformation of the human telomeric DNA. This folding structure has also been independently reported by two other groups (24,25). We continue our previous work to determine its molecular structure in solution by NMR, and to delineate the important/unique features of the human telomeric G-quadruplex in K^+. Here, we report the NMR solution structure of this physiologically relevant hybrid-type human telomeric G-quadruplex. Our study provides not only the molecular details of this telomeric G-quadruplex, but also important insights into its loop conformations and their interactions with the core tetrad structures. Significantly, a novel adenine triple capping structure is found to form, covering one end of the telomeric G-quadruplex, which is likely to play an important role in the formation of the stable telomeric G-quadruplex structure in K^+.

An NMR solution structure has very recently been reported on the human telomeric G-quadruplex in K^+ (25). Our structure differs from the previously reported structure in several aspects. First, our results show substantial differences in the loop conformations and their specific interactions with the core G-tetrads. Second, the structure reported here uniquely provides the molecular basis for design of drugs that target the physiologically relevant human telomeric G-quadruplex.

MATERIALS AND METHODS

Sample preparation

The DNA oligonucleotides were synthesized using β-cyanoethylphosphoramidite solid-phase chemistry on an Expedite™ 8909 Nucleic Acid Synthesis System (Applied Biosystem, Inc.) in DMT-on mode, and were purified using C18 reverse-phase HPLC chromatography, as described earlier (23,26–28). Samples in D_2O were prepared by repeated lyophilization and final dissolution in 99.96% D_2O. Samples in water were prepared in 10%/90% D_2O/H_2O solution. The final NMR samples contained 0.1–2.5 mM DNA in 25 mM K-phosphate buffer (pH 7.0) and 70 mM KCl.

NMR experiments

NMR experiments were performed on a Bruker DRX-600 spectrometer as described earlier (23,26,29). Standard 2D NMR experiments, including NOESY, TOCSY and DQF-COSY, were collected at 1, 7, 15, 20, 25, 30 and 35°C to obtain the complete proton resonance assignment. Non-exchangeable protons were estimated based on the NOE cross-peak volumes at 50–300 ms mixing times, with the upper and lower boundaries assigned to ±20% of the estimated distances. Distances between exchangeable protons were assigned with looser boundaries of ±20–30%. The base methyl proton (Me)-H6 distance (2.99 Å) was used as a reference. The distances involving the unresolved protons, e.g. methyl protons, were assigned using pseudo-atom notation to make use of the pseudo-atom correction automatically computed by X-PLOR.

The ^{31}P NMR spectra, including 2D ^{31}P–^{1}H COSY and HSQC, were collected on a 2.5 mM DNA sample in D_2O at 25°C and were referenced to an external standard of 85% H_3PO_4, as described earlier (26). Various heteronuclear INEPT transfer delays corresponding to J-couplings of 7, 10, 15, 20 and 25 Hz, were used for a series of ^{31}P–^{1}H HSQC.

Distance geometry and simulated annealing (DGSA) calculations

Metric matrix distance geometry (MMDG) and simulated annealing calculations were carried out in X-PLOR (30) to embed and optimize 100 initial structures based on an arbitrary extended conformation of the single-stranded Tel26 sequence, as described earlier (26). The experimentally obtained distance restraints and G-tetrad hydrogen-bonding distance restraints were included during the calculation.

NOE-distance restrained molecular dynamics calculations

All of the 100 molecules obtained from the DGSA calculations were subjected to NOE-restrained simulated annealing refinement in XPLOR (30) with a distance-dependent dielectric constant, as described earlier (26). Each individual hydrogen bond was restrained using two distance restraints (heavy atom–heavy atom and heavy atom–proton). Looser hydrogen-bonding distance restraints were applied to the A25:T14 base pair, with larger distance boundaries (±0.4 Å). The force constants were scaled at 30–60 and 100 $kcal \cdot mol^{-1} \cdot Å^{-2}$ for NOE and hydrogen bond distance restraints, respectively. All distance restraints were specified with the SUM averaging option in X-PLOR (30). A total of 552 NOE distance restraints, of which 279 are from inter-residue NOEs, were incorporated into the NOE-restrained structure calculation.

Dihedral angle restraints were used to restrict the glycosidic torsion angle (χ) for the experimentally assigned *syn* conformation bases, including G4, G10, G16, G17 and G22 tetrad-guanines, and the 5′-terminal A1 [60(±35)°], and for the experimentally assigned G-tetrad *anti* conformation bases, including G5, G6, G11, G12, G18, G23 and G24 [240(±40)°]. Dihedral angle restraints were also used to restrain some sugar backbone torsion angles ε based on the ^{31}P–^{1}H coupling constants, as described earlier (26). The $^{3}J_{H3'P3'}$-coupling constants were obtained from ^{31}P–^{1}H COSY and confirmed by HSQC experiments using various J-coupling delays. A $^{3}J_{H3'P3'}$-coupling constant larger than 15 Hz is indicative of an ε angle in the *gauche*+/*trans*+ region 60 ± 50°, while a H3′(n)–^{31}P($n+1$) coupling constant smaller than 10 Hz is indicative of an ε angle '*not*' in the 60 ± 50° region, i.e. 110–370°; however, the values cannot be more accurately determined due to the existence of several possible ε angles for a single $^{3}J_{H3'P3'}$-coupling in this region (31). The ε angles restraints are 60(±40)° for G4, T8, A9, T20, A26 ($^{3}J_{H3'P3'}$ >20 Hz); 60(±50)° for T19 and G22 ($^{3}J_{H3'P3'} > 15$ Hz); 60(±60)° for T14 and G16 ($^{3}J_{H3'P3'} \geq 15$ Hz), and 240(±145)° for T7, G10, T13 and A15 ($^{3}J_{H3'P3'} < 10$ Hz). The force constants of dihedral

angle restraints were 10 kcal·mol^{-1}·rad^{-2} for χ and 5 kcal·mol^{-1}·rad^{-2} for ε.

NOE-restrained simulated annealing refinement calculations were performed as described earlier (26). The time steps for all processes of heating, cooling and equilibration were equal to 1 fs. The 10 best molecules were selected based both on their minimal energy terms and number of NOE violations and have been deposited in the Protein Data Bank (PDB ID 2HY9).

RESULTS

The hybrid-type mixed parallel–antiparallel-stranded folding pattern of the major intramolecular human telomeric G-quadruplex in K^+ solution

We have recently shown that the major intramolecular telomeric G-quadruplex in potassium solution adopts a novel hybrid-type mixed parallel–antiparallel-stranded G-quadruplex using a 26-nt sequence Tel26 (Figure 1A) (23). Tel26 contains the wild-type 22-mer four-repeat human telomeric sequence d[AGGG(TTAGGG)$_3$] (Tel22) (Figure 1A), which has been used for a number of previous studies (24,32–34), plus a flanking AA at each end. The imino region of the 1D ^{1}H NMR spectrum of Tel26 in K^+ is shown in Figure 1B, with 12 well-resolved imino proton resonances. The base imino and H8 protons of 12 guanine residues have been unambiguously assigned by site-specific low-enrichment (6%) using 1, 2, 7-^{15}N, 2-^{13}C-labeled guanine nucleoside at each guanine position of the sequence (Figures 1B and S1) (23). The assignment of the guanine imino and H8 protons leads to the direct determination of the folding topology of the telomeric G-quadruplex in K^+ solution (Figure 1C). The first, second and fourth G-strands of this hybrid-type G-quadruplex are parallel with each other, and antiparallel with the third G-strand. The first two G-strands (from the 5′-end) are linked with a TTA double-chain-reversal side loop, while the second, third and fourth strands are linked with two TTA lateral loops. Tel26 has been shown to exhibit the same CD spectral signature as the WT-Tel26 sequence, strongly suggesting that they adopt the same major conformation in K^+ solution (23). The NMR melting-temperature titration experiment showed that this major G-quadruplex formed in Tel26 in K^+ (sharp peaks in Figure 1B) is unimolecular (Figure S2A) (23). The NMR spectra of Tel26 at a strand concentration of 2.5 mM (for 2D NMR experiments and structure determination) and 0.6 mM (for 1D experiments and the titration experiment) are the same, indicating that the same monomeric intramolecular G-quadruplex structure is formed in all the conditions used for our NMR analysis (Figure S2B). Minor conformations are also present as indicated by the presence of weak resonances, whose intensities are <10% of the major species and thus do not interfere with the unambiguous structural analysis of the predominant telomeric G-quadruplex structure. We have examined our NMR sample using mass spectrometry and EMSA experiments (data not shown). No higher molecular weight component was found in our sample.

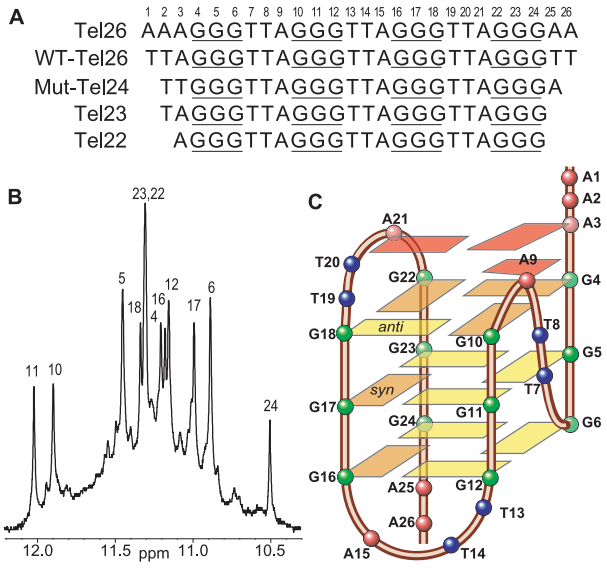

Figure 1. (**A**) Different four-repeat human telomeric DNA sequences. WT-Tel26, Tel22 and Tel23 are the wild-type four-repeat telomeric DNA sequences with sizes of 26-, 22- and 23-nt, respectively. Mut-Tel24 is the modified sequence used in the recent report (25). The numbering system is shown above Tel26. (**B**) The imino proton region of the 1D ^{1}H NMR spectrum of Tel26 in K^+ with assignment. (**C**) Schematic drawing of the folding topology of the unimolecular human telomeric G-quadruplex in K^+ solution. The three naturally occurring adenine residues involved in the adenine triple capping structure are shown in red. Yellow box = (*anti*) guanine, orange box = (*syn*) guanine; green ball = guanine, red ball = adenine, blue ball = thymine.

2D NMR experiments provide ^{1}H and ^{31}P assignments for the human telomeric G-quadruplex in K^+

We were able to assign all proton resonances for the telomeric G-quadruplex in K^+ using multiple 2D NMR experiments, including 2D-NOESY, TOCSY and COSY. Standard DNA sequential assignment procedure was utilized for the assignment of the non-exchangeable protons (Figures 2A and S3). The base H6 proton resonances of thymines have been unambiguously assigned by substituting deoxyuridine (dU) for dT at each thymine position of Tel26. The assignment of the aromatic protons allowed the direct assignment of H1′ and H2′/H2″ protons, and was then extended to H3′, H4′ and H5′/H5″. All proton resonances have been unambiguously assigned, except some H5′/H5″ protons which cannot be differentiated. The proton chemical shifts at 25°C are listed in Table 1. As there are clearly minor species, we have spent particular effort to obtain an accurate assignment and structure calculation. We have collected data at various temperatures, 1, 7, 15, 20, 25, 30 and 35°C, with multiple mixing times, in both D_2O and H_2O, as the chemical shifts are not only temperature-dependent but also solvent-dependent. The complete spectral assignment was achieved by examining all these spectra at different conditions. We made sure that the same NOE assignment pathway and the connectivities with the adjacent residues for the major conformation can be followed at all experimental conditions. For weak NOE

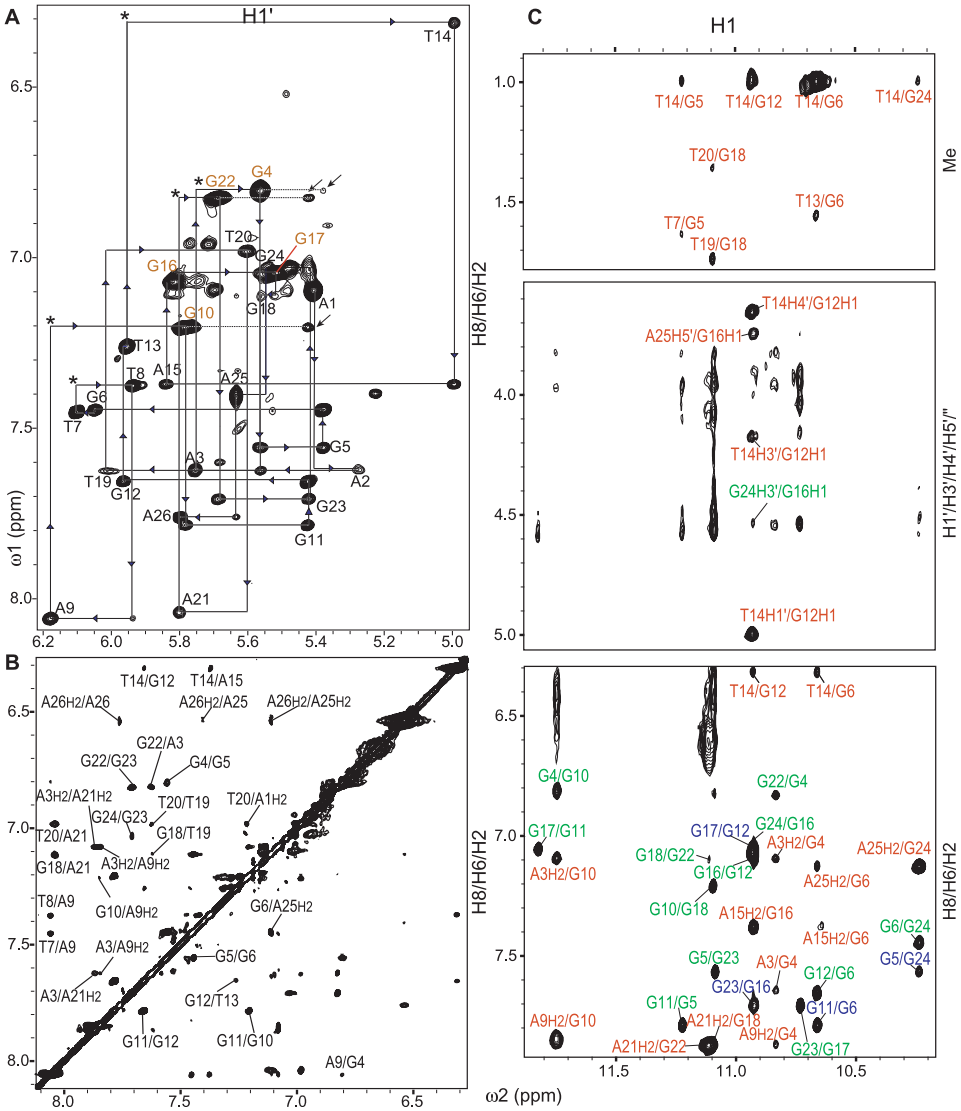

Figure 2. The expanded H8/H6–H1′ region (**A**) and aromatic–aromatic region (**B**) of the non-exchangeable 2D-NOESY spectrum of Tel26 in K^+ solution. In (A), the sequential assignment pathway is shown. Missing connectivities are labeled with asterisks. The three peaks, A1H1′/A2H8, T19H1′/T20H8, T20H1′/A21H8, that appear to be missing but are not labeled are observable at a lower contour level, and are related with a broader linewidth. The H8-H1′ NOEs of the nucleotides in *syn* conformation are labeled in orange, while the H8-H1′ NOEs of the nucleotides in *anti* conformation are labeled in black. The characteristic G(*i*)H8/G($i+1$)H1′ NOEs for the *syn* G(*i*)s are labeled by arrows. In (**B**), the H2 protons are specified. (**C**) The expanded imino regions of the exchangeable proton 2D JR-NOESY spectrum of Tel26 in K^+ solution. NOEs between loop residue protons and G-tetrad imino protons are labeled in red, intra-tetrad NOEs are labeled in green and inter-tetrad NOEs are labeled in blue. In the bottom panel, the aromatic H2 protons are specified. Conditions: 1°C, 25 mM K-phosphate pH 7.0, 70 mM KCl, 2.5 mM DNA.

peaks, only those that could be consistently observed at all different conditions and that follow the same connectivities with the flanking residues were used for assignment, structure determination and calculation.

Using 2D ^{31}P–^{1}H COSY (Figure 3) and ^{31}P–^{1}H HSQC, combined with the proton assignments, we were also able to unambiguously assign all of the ^{31}P resonances (Table 1). A phosphorus resonance was assigned by using the assignments of sugar protons H3′, H4′ and H5′/H5″, and by correlating it to its 5′-coupled H3′ proton and 3′-coupled H4′ and H5′/H5″ protons. Moreover, the phosphorus assignments confirmed the proton assignments of H3′ ($n-1$), H4′ (n) and H5′/H5″(n) for each step. While the majority of the ^{31}P resonances of the telomeric G-quadruplex are clustered around -1 ± 0.5 ppm, as observed for regular right-handed B-DNAs, a number of ^{31}P resonances are shifted outside this region, with those of the G12-T13 and T14-A15 steps of the second TTA lateral loop being the most shifted (Table 1).

Inter-residue NOEs define the overall structure of the telomeric G-quadruplex in K^+

Many inter-residue NOEs are observed in 2D-NOESY of Tel26 in K^+ (Figure 2). Critical inter-residue NOEs are schematically summarized in Figure 4. These NOEs

define the overall structure of the telomeric G-quadruplex in K^+, as discussed in more detail below. The majority of residues, except for G6, G11 and A25, have resolved H2′ and H2″; while for each residue, the H1′–H2″ NOE is stronger than H1′–H2′ and the H3′–H2″ NOE is close to or weaker than H3′–H2′, indicating a C2′-*endo* sugar pucker conformation.

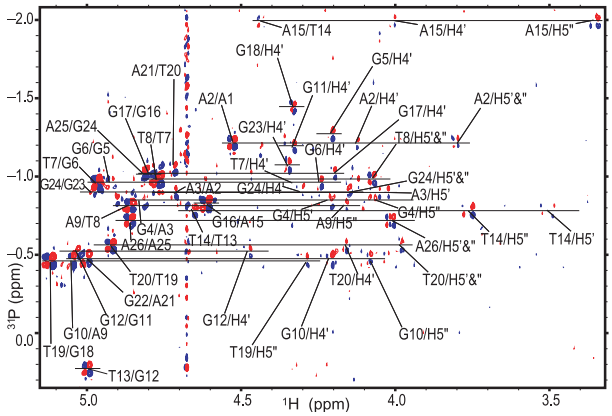

Figure 3. 2D heteronuclear ^{31}P–^{1}H Correlation Spectroscopy (COSY) of Tel26 in K^+ solution with peak assignments. The (n)P–$(n-1)$H3′ peaks are labeled as 'residue name (n)/residue name $(n-1)$,' while the (n)P–(n)H4′ or (n)P–(n)H5′,″ peaks are labeled as 'residue name/H4″' or 'residue name/H5′,″', respectively. The spectra were referenced to external H_3PO_4. Conditions: 25°C, 25 mM K-phosphate, 70 mM KCl, pH 7.0, 2.5 mM DNA.

NOEs of the core G-tetrads define the mixed G-arrangements for the telomeric G-quadruplex in K^+

Five guanine residues of the core G-tetrads are in the *syn* conformation, including G4, G10, G16, G17 and G22 (Figure 1C), as indicated by the very strong H8–H1′ NOE intensities (Figures 2A and S3). A characteristic downfield shift is observed for the H2′/H2″ sugar protons of the *syn*-guanines (Table 1). The regular sequential NOE connectivities are either missing or very weak at the N(i)-*syn*G($i+1$) steps i.e. A3–G4, A9–G10, A15–G16, G16–G17 and A21–G22 (Figures 2A and S3). In addition, the characteristic *syn*G(i)H8/G($i+1$)H1′ NOEs are observed for G4–G5, G10–G11, G17–G18 and G22–G23 (Figure 2A). In contrast, for the N(i)-*anti*G($i+1$) steps, the sequential NOE connectivities are clearly observed, such as between the base H8 protons and its 5′-flanking residues' sugar H1′/H2′/H2″ protons, typical for right-handed DNA (Figures 2A and S3). As shown in Figure 1C, the bottom two G-tetrads of the hybrid-type telomeric G-quadruplex have the same (*anti:anti:syn:anti*) G-arrangement, while the first G-tetrad has a reversed (*syn:syn:anti:syn*) G-arrangement. The guanine distribution of the three parallel G-strands (first, second and fourth) is (5′-*syn-anti-anti*), while that of the antiparallel G-strand (third) is reversed, (5′-*anti-syn-syn*). In accord with the topology, the reversed G-arrangements of the top two G-tetrads are clearly reflected by strong inter-strand, inter-tetrad NOEs of guanine imino protons, such as G4H1/G23H1,

Table 1. ^{1}H and ^{31}P chemical shifts for Tel26 in K^+ at 1°C[a]

	H6/H8	NH1/NH3 H2/Me	NH21/NH22 NH61/NH62	H1′	H2′, H2″	H3′	H4′	H5′, H5″	^{31}P[b]
A1	7.10	7.22		5.41	1.63, 1.96	4.28	3.62	3.04, 2.96	
A2	7.60	7.17		5.27	1.94, 2.16	4.50	3.89	3.58	−1.22
A3	7.62	7.08	6.40, –	5.75	2.33, 2.41	4.53	4.03	3.74, 3.82	−0.90
G4[c]	6.80	10.84	8.92, –	5.56	2.90, 2.52	4.57	4.09	3.82, 3.95	−0.84
G5	7.56	11.22	6.08, 9.55	5.38	2.18, 2.26	4.66	3.95	3.82, 3.87	−1.27
G6	7.45	10.66		6.05	2.24	4.68	4.03	3.75, 3.82	−0.96
T7	7.45	1.63		6.10	2.13, 2.23	4.52	4.04	3.72, 3.85	−0.96
T8	7.38	1.71		5.93	1.88, 2.18	4.60	4.02	3.82	−0.98
A9	8.06	7.85		6.18	2.61, 2.55	4.82	4.24	3.83, 3.93	−0.81
G10	7.20	11.75	6.44, 9.15	5.78	3.12, 2.76	4.76	4.10	3.82, 3.97	−0.46
G11	7.79	11.82	5.76, 9.87	5.42	2.34	4.79	4.08	3.94, 4.05	−1.18
G12	7.66	10.93		5.96	2.37, 2.25	4.74	4.24	3.94, 3.98	−0.51
T13	7.26	1.55		5.96	2.08, 2.16	4.41	3.90	3.76, 3.85	0.24
T14	6.31	1.00		5.00	0.96, 1.78	4.17	3.65	3.27, 3.53	−0.78
A15	7.37	7.38		5.84	1.96, 2.22	4.35	3.73	2.46, 3.09	−2.00
G16	7.07	10.92		5.81	3.16, 2.67	4.54	4.14	3.90, 4.01	−0.82
G17	7.04	10.73	6.00, 9.33	5.52	2.18, 2.30	4.67	3.96	3.93, 4.03	−1.04
G18	7.11	11.09		5.56	2.29	4.84	4.07	3.90	−1.46
T19	7.63	1.74		6.01	2.11, 2.27	4.66	4.19	3.88, 4.07	−0.46
T20	6.98	1.36		5.60	1.07, 2.06	4.49	3.92	3.76	−0.55
A21	8.04	7.87		5.80	2.50, 2.44	4.75	4.13	3.67, 3.81	−1.05
G22	6.82	11.12	6.58, 8.06	5.69	3.08, 2.58	4.68	4.17	3.93, 4.05	−0.47
G23	7.71	11.09	5.50, 9.30	5.42	2.28, 3.32	4.73	4.10	3.90, 3.98	−1.08
G24	7.03	10.24	5.40, 8.47	5.53	1.79, 2.13	4.53	4.06	3.91	−0.90
A25	7.41	7.11		5.63	2.12, 2.17	4.59	3.96	3.75, 3.79	−1.02
A26	7.76	6.54		5.80	2.56, 2.07	4.26	3.81	3.77, 3.75	−0.71

[a]The chemical shifts are measured in 25 mM K-phosphate, 70 mM KCl, pH 7.0, referenced to DSS.
[b]The ^{31}P chemical shifts are measured at 25°C and referenced to H_3PO_4.
[c]Guanines in *syn* glycosidic conformation are in bold.

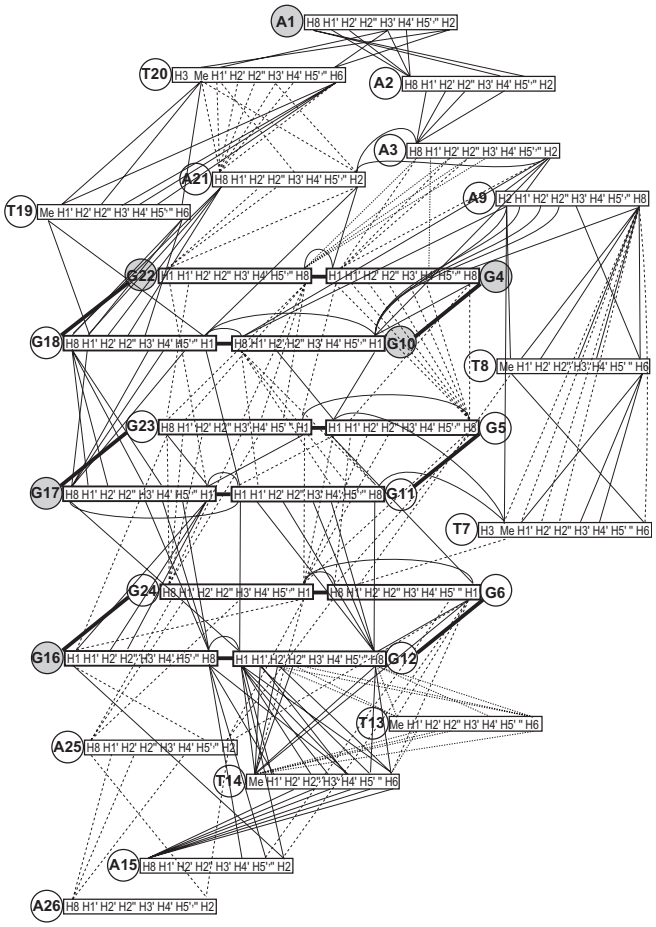

Figure 4. Schematic diagram of inter-residue NOE connectivities of Tel26 G-quadruplex formed in K^+ solution. The guanines in *syn* conformation are represented using gray circles. The NOE connectivities clearly define the G-quadruplex conformation and provide distance restraints for structure calculation.

G10H1/G5H1, G18H1/G11H1 and G22H1/G17H1 (Figure S4); while the same G-arrangements of the bottom two G-tetrads are reflected by H8/H8 and H1/H1 NOEs between adjacent guanines, i.e. G5–G6, G11–G12, G16–G17 and G23–G24 (Figures 2B and S4). Furthermore, the right-handedness of G-strands is indicated by NOEs between the bottom two G-tetrads, e.g. G6H1/G11H8, G12H1/G17H8, G16H1/G23H8 and G24H1/G5H8 (Figure 2C).

NOEs of loop regions define the unique loop conformations, especially the formation of a novel adenine triple capping structure, for the telomeric G-quadruplex in K^+

All residues in the loop regions are in the *anti* conformation except A1, which shows a strong H8-H1′ NOE (Figures 2A and S3). Many inter-residue NOEs are observed for the three loops (Figure 4), which define the unique loop conformations and their specific interactions with the core G-tetrads in the telomeric G-quadruplex in K^+. In particular, a novel adenine triple structure is found to form using three naturally occurring adenine residues, capping one end of the telomeric G-quadruplex. The details of the loop conformations are described below.

A capping structure of adenine triple is formed by three naturally occurring residues, A3, A9 and A21, at the 5′-end of the telomeric G-quadruplex in K^+

A novel capping structure was found to form using three naturally occurring adenine residues, A3, A9 and A21, and covers the top G-tetrad (Figures 4 and 1C) of the human telomeric G-quadruplex in K^+. The A3 residue in the 5′-flanking segment (Figure 1C), which is a naturally occurring residue in the human telomeric sequence, appears to stack very well with the top G-tetrad (Figure 4). A number of NOEs are observed between A3 and G4(*syn*), indicating that A3 stacks over the G4 base. In addition, a number of NOEs are observed between the H8/sugar protons of A3 and G22H8 (Figures 2B and 4), as well as a relatively strong NOE between A3H2 and G10H1 (Figure 2C). These NOEs place the A3 base right above the G4 base with A3H2 pointing towards the G10 direction (Figure 1C). The other two residues in the 5′-flanking segment, A1 and A2, are both mutations from the wild-type sequence (Figure 1C). NOEs of the A1 and A2 residues (Figure 4) indicate that while A2 stacks over A3, A1 adopts a *syn* conformation and is positioned above A2 and the T20 of the third TTA lateral loop.

Interestingly, the A9 residue in the first TTA double-chain-reversal side loop (Figure 1C) appears to be positioned above the top G-tetrad as well. A number of NOEs are observed between A9 and the top G-tetrad (Figure 4). A9H2 shows a relatively strong NOE interaction with G10H1 (Figure 2C) and a weaker NOE with G10H8 (Figure 2B). A9H8 shows a clear NOE with G4H8 (Figure 2B). The NOEs between the sugar protons of A9 and the H8 of G10 are missing due to the *syn* conformation of G10, however, G10H1 has weak NOEs with the A9 sugar protons (Figure 4). These NOEs define the position of the A9 base, which is above the G10:G4 edge of the top tetrad (Figure 1C). The lack of NOEs between A9H2 and G4H8 or the G10 sugar protons, or between A9H8 and the G10 sugar protons, eliminates the possibility of the A9 base positioning in the groove. The other two residues in the first TTA loop, T7 and T8, appear to be positioned in the groove. Regular sequential NOEs are more or less observed for the T8–A9 step (Figure 4). However, sequential NOE connectivities are either missing or very weak at the T7–T8 step, while some unusual NOEs are observed between T7 and A9 (Figure 4). In addition, a number of NOEs are observed for T7 with the core G-tetrads (Figure 4), including a relatively strong NOE of T7Me/G6H1′, weaker NOEs of T7Me/G5H1 and T7Me/G11H8, whereas only one clear NOE of T8Me/G6H1′ is observed for T8 with the core G-tetrads, indicating that T7 is positioned closer to the core G-tetrads and closer to the second G-run (G10–G11–G12).

The A21 residue in the third TTA lateral loop (Figure 1C) also appears to stack very well with the top G-tetrad. Strong NOEs are observed between A21H2 and G18H1 (Figure 2C), A21H8 and G18H8 (Figure 2B), as well as between A21H8 and sugar protons of G18 (Figure 4), indicating that A21 stacks right on the G18 of the top tetrad (Figure 1C). In addition, G22H1

shows clear NOEs with A21H2 (Figure 2C) and A21H2′/H2″ (Figure 4). T20 in this lateral TTA loop appears to stack quite well with A21, as indicated by sequential NOE connectivities between A21 and T20 (Figure 4). A closer positioning of T20 and A21, typical for loop residues, is indicated by a relatively strong NOE interaction between T20H1′ and A21H3′ (Figure 4). Weaker NOEs are observed between the H6/Me base protons of T20 and the sugar protons of T19 (Figures 2A and 4). Whereas other sequential B-DNA NOEs are missing at the G18–T19 step (Figure 4), two relatively strong NOEs are observed between G18H1′ and the base protons H6 and Me of T19, suggesting that the T19 base is positioned in the groove close to G18H1′.

Furthermore, there are a number of important NOEs observed between A3 and A21, and between A3 and A9 (Figure 4), indicating the formation of the adenine triple. For example, A9H2 shows a relatively strong NOE with A3H2 (Figure 2B), and A9H1′ shows a weak NOE with A3H2 (Figure 4). Therefore, the H2 end of A9, which is above the G10:G4 edge of the top tetrad, is pointing towards A3 (Figure 1C). In addition, clear NOEs are observed for A21H2 with both the A3H2 and A3H8 (Figure 2B). It is interesting to note that similar upfield-shifting is observed for the base and sugar protons of both the A9 and A21 residues (Figure 2, Table 1).

The second TTA lateral loop and the 3′-flanking segment cover the bottom end of the telomeric G-quadruplex in K^+

The NOE data indicate that T14 of the second TTA lateral loop (Figure 1C) stacks completely underneath the bottom G-tetrad while T13 is looped out. An unusually large number of NOEs are observed between T14 and G12 (Figure 4). For example, the base methyl and H6 protons of T14 show clear NOEs with the base H1 and H8 protons of G12 (Figure 2B and C), and T14 methyl also show clear NOEs with the sugar H1′, H2′,″ protons of G12 (Figure 4). G12H1 shows clear NOEs with the H1′ and H4′ sugar protons of T14 (Figure 2C). In addition, clear NOEs are observed for G6H1 with T14Me (strong) and T14H6 (medium) (Figure 2C). Thus T14 appears to stack underneath the bottom G-tetrad and is completely covered by the G12 base. This is supported by the markedly upfield-shifted chemical shifts of the base and sugar protons of T14 as well as the H5′/H5″ protons of A15 (Table 1), likely due to the ring-current effect of the G12 base. For the looped-out T13, regular sequential NOEs between T13H6 and its 5′-flanking G12 are missing or very weak (Figures 2A and S3). NOEs are observed between G12H8 and the sugar protons of T13, indicating a somewhat left-handed conformation for the G12–T13 step. T13 is poorly stacked with T14, as indicated by the very weak NOEs between T13 and T14 (Figures 2A and S3). Sequential NOE connectivities for right-handed DNA conformation are clearly observed at the T14–A15 step; however, such NOEs are weak at the A15–G16 step (Figure 4). A number of unusual NOEs are observed between the sugar protons of T14 and A15 (Figure 4), suggesting the sugar moieties of the two residues are in close proximity. A15H2 shows clear NOEs with the imino protons of G12 and G16 (Figure 2C), indicating that A15 is stacked below the bottom G-tetrad.

Sequential NOE connectivities are clearly observed within the 3′-terminal G24–A25–A26 flanking segment (Figure 4), indicating a stacked conformation within this region. A25 stacks very well with the bottom G-tetrad, and is positioned right underneath G24 and G6 (Figure 1C), as indicated by the relatively strong NOEs of A25H2 with G6H8 (Figure 2B), as well as with G24H1 and a weaker NOE with G6H1 (Figure 2C).

NMR structure calculation

NOE experimental data (Figure 4) define the overall structure of telomeric G-quadruplex in K^+ and were applied for NMR structure calculation using a NOE-restrained distance geometry (DGSA) and molecular dynamics (RMD) approach, starting from an arbitrary extended single-stranded DNA. A total of 552 NOE distance restraints, of which 279 are from inter-residue NOEs, were incorporated into the NOE-restrained structure calculation (Table 2). Very few NOEs associated with H5′ or H5″ were used for structure calculation, due to possible ambiguities associated with H5′ or H5″ protons. Dihedral angle restraints were used for the glycosidic torsion angle (χ) for all the experimentally determined *syn* residues, and for the *anti* guanines. Dihedral angle restraints were also applied for a number of unusual torsion angles ε based on the $^3J_{H3'P3'}$-couplings to better define the loop conformations (see MATERIALS AND METHODS section). It is interesting to note that the residues exhibiting unusually large $^3J_{H3'P3'}$-coupling constants are all associated with the loop regions, i.e. ~20 Hz for T7–T8, T8–A9, T13–T14, T19–T20 and A21–G22 steps; and ~15 Hz for G12–T13, T14–A15, A15–G16 and G18–T19 steps.

Table 2. Structural statistics for Tel26 in K^+[a]

NMR distance and dihedral constraints	
Distance restraints	
Total NOE	552
Intra-residue	273
Inter-residue	279
Sequential($\|i-j\|=1$)	186
Non-sequential($\|i-j\|>1$)	93
Hydrogen bonds	26
Total dihedral angle restraints	27
Structure statistics	
Violations (mean and SD)	
Distance constraints (>0.2 Å)	5.73 ± 2.10
Dihedral angle constraints (>6°)	0
RMSD of distance violation (Å)	0.054 ± 0.002
RMSD of dihedral angle violation (°)	1.22 ± 0.16
Deviations from idealized geometry	
Bond length (Å)	0.009 ± 0.0003
Bond angle (°)	1.61 ± 0.008
Impropers (°)	1.18 ± 0.01
RMSD of all atoms (Å)	
G-tetrads	0.69 ± 0.07
Residues 3–25	0.91 ± 0.09
All residues	1.22 ± 0.16

[a]The ensemble of 10 structures is selected based both on the minimal energy terms and number of NOE violations.

The superimposition of the 10 lowest energy structures produced by the NOE-restrained structure calculation is shown in Figure 5 (PDB ID 2HY9). The structure statistics are listed in Table 2. Remarkably, the telomeric G-quadruplex structure is very well defined, including the three TTA loops (Figure 5). For the 10 lowest energy structures, the RMSD is 1.22 Å for all residues, and only 0.91 Å for residues 3–25, including the 5′-flanking A3, three TTA loops and the 3′-flanking A25. The RMSD is 0.69 Å for the three core G-tetrads (Table 2).

Molecular structure of the human telomeric G-quadruplex structure in K^+

A representative molecular model of the human telomeric G-quadruplex formed in K^+ solution is shown in two different views in Figure 6. This hybrid-type mixed parallel–antiparallel-stranded G-quadruplex contains three well-defined G-tetrads and four grooves of different widths, with two intermediate (grooves I and IV), one wide (groove II) and one narrow (groove III) (Figure 6). All the δ torsion angles fall in the range of 110–150°, consistent with the C2′-endo sugar pucker conformations indicated by the NMR data. As observed earlier (26), extensive stacking between the guanine five-membered rings is observed for the top two G-tetrads whose adjacent guanines have the reversed glycosidic conformations, while only partial stacking is observed for the bottom two G-tetrads whose adjacent guanines have the same glycosidic conformations (Figure S5).

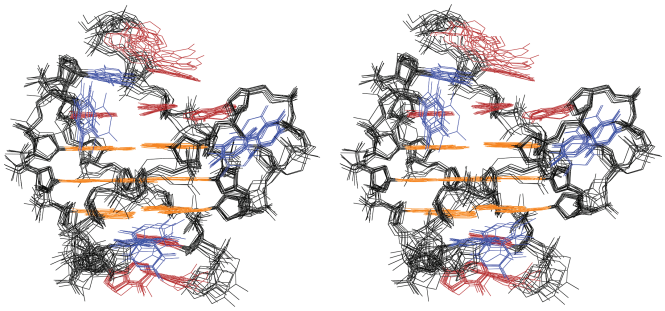

Figure 5. Stereo view of the superimposed 10 lowest energy structures of the Tel26 G-quadruplex in K^+ solution by NOE-restrained structure refinement (guanine base = orange, adenine base = red, thymine base = blue).

As shown in Figure 5 and Table 2, the three TTA loops of the human telomeric hybrid-type G-quadruplex in K^+ are well defined, including the first TTA loop segment (T7–T8–A9) which adopts a double-chain-reversal loop conformation. The loop conformations are in good agreement with the experimental NMR data (Figure 4). The A9 residue of the first TTA loop is positioned above the top G-tetrad, right outside the G10:G4 edge, and participates in the adenine triple capping structure (Figure 6). Both T7 and T8 are positioned in groove I in a triangle arrangement with A9, while T7 is closer to the core tetrads and the second G-strand (G10–G11–G12) (Figure 7A). T8 is somewhat stacked with A9, but very little stacking is observed between T8 and T7, consistent with the missing connectivities between T7 and T8 (Figure 2A). The second and third TTA loop segments adopt well-defined lateral loop conformations (Figure 7B and C). A21 of the third TTA loop (T19–T20–A21) is very well stacked with the G18 of the top G-tetrad. T20 is stacked over A21. T19 is looped out with its base lying in groove II (Figure 7B), in accord with the strong NOEs between G18H1′ and T19H6 (Figure 2A) and T19Me .

In addition, the A3 of the 5′-flanking segment is very well stacked with the top G-tetrad as well, with its base pointing towards G10 (Figure 6). The very well stacked A21 and A3 constitute the core of the adenine triple structure capping the top end of the hybrid-type telomeric G-quadruplex in K^+. The formation of this unique adenine triple platform can be clearly seen in Figure 8A. The three adenines, A21, A3 and A9, involved in the adenine triple formation are all naturally occurring residues in the human telomeric sequence. While all three adenines stack with the top G-tetrad, A21 and A3 have more extensive stacking, while A9 is positioned more towards the outside of the top tetrad. A potential hydrogen bond could be formed between the amino proton A3H62 and A21N1, whose distance is ~2.05 Å, as

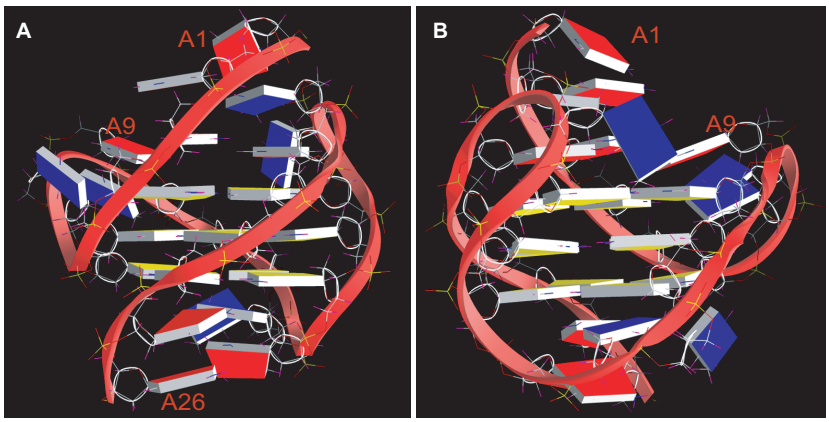

Figure 6. A representative model of the NMR-refined Tel26 G-quadruplex structure from two different views, prepared using GRASP (35) (guanine = yellow, adenine = red, thymine = blue).

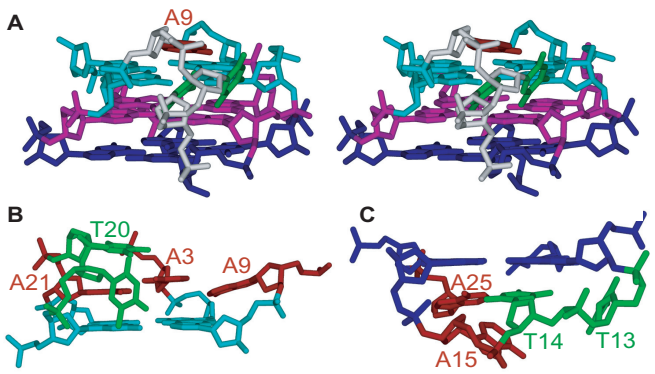

Figure 7. Loop conformations in the Tel26 quadruplex in K^+ solution. (**A**) Stereo views of the first TTA loop (T7–T8–A9) which adopts a double-chain-reversal loop conformation. (**B**) Loop interactions with the top G-tetrad. The unique adenine triple capping structure is shown. The third T19–T20–A21 lateral loop is also shown. (**C**) Loop interactions with the bottom G-tetrad. The second T13–T14–A15 lateral loop is shown. The loop adenines are in red, while the loop thymines are in green. The top G-tetrad (as in Figure 1C) is in cyan, the middle G-tetrad is in magenta and the bottom G-tetrad is in blue.

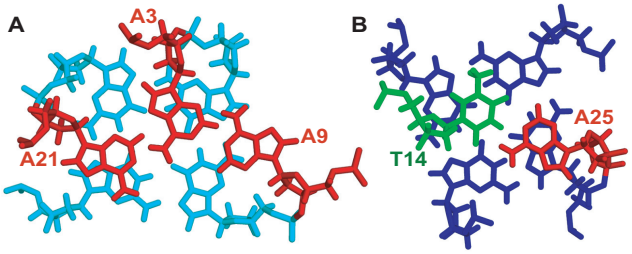

Figure 8. (**A**) The top view of the adenine triple (red) capping the top G-tetrad (cyan). The distance is 2.05 Å for A3H62/A21N1, and 2.27 Å for A21H2/A3N7, respectively. (**B**) The bottom view of the A25:T14 base pair (adenine in red and thymine in green) capping the bottom G-tetrad (blue). Figures are prepared using PyMOL.

a strong NOE is observed between A3H62 and A21H2 (Table 1) at 1°C.

The second TTA lateral loop (T13–T14–A15) covers the bottom end of the telomeric G-quadruplex, with T14 positioned completely underneath G12 and T13 looped out (Figure 7C), in accord with the missing connectivities between T13 and T14 (Figure 2A). Moreover, A25 from the 3′-flanking segment is very well stacked with the bottom G-tetrad (Figure 6). Potential reversed Watson–Crick hydrogen bonds could be formed between T14 and A25 (Figure 8B), as a weak imino proton resonance, likely to be T14H3, was observed at low temperatures for Tel26 (data not shown). However, it needs to be noted that A25 is a mutated residue from the native thymine in the human telomeric sequence.

DISCUSSION

Our results show the molecular details of the major telomeric G-quadruplex formed in K^+ solution, a hybrid-type mixed parallel–antiparallel-stranded G-quadruplex structure. A report has very recently appeared (25) on the telomeric G-quadruplex structure in K^+. Our structure differs substantially from the structure reported in this previous report (25). The important adenine triple capping structure was not recognized and the 5′-TTA double-chain-reversal loop was not well defined in this recent report. Unfortunately, the critical native 5′-flanking adenine was mutated to a thymine in their sequence for structure determination (Figure 1A) (25). As described in the Results section, our structure was determined based on a full array of experimental NMR data and has been shown to agree well with all the experimental data, including NOE and NMR correlation results. In contrast, this previous report lacks this information (25); it is therefore difficult to make a complete comparison.

Our NMR solution structure of the human telomeric hybrid-type G-quadruplex in K^+ solution is very well defined (Figure 5), as demonstrated by the small RMSD values of the 10 lowest energy structures, e.g. the RMSD for the core G-tetrads is only 0.69 Å (Table 2). Significantly, the three TTA loops and the two flanking segments are also very well defined, as indicated by a RMSD value of 0.91 Å. The 5′-flanking segment, the third TTA lateral loop and the A9 residue of the first TTA double-chain-reversal side loop, cover the top end of the telomeric G-quadruplex. The second TTA lateral loop together with the 3′-flanking segment, cover the bottom end of the telomeric G-quadruplex. Our study indicates that the three loop regions and the two flanking segments all interact with the core G-tetrads in a specific way that defines and stabilizes the unique human telomeric G-quadruplex structure in K^+.

A significant feature we found in our structure is the formation of a well-defined novel adenine triple structure by three naturally occurring adenine residues, A21, A3 and A9, capping the top tetrad of the hybrid-type telomeric G-quadruplex (Figure 8A). Significantly, the top tetrad covered by the adenine triple consists of three *syn* guanines and one *anti* guanine. The G-tetrad containing more *syn* guanines is known to be less stable than the G-tetrad containing more naturally occurring *anti* guanines, and thus requires a capping structure for additional stabilization. For example, in the recently determined major G-quadruplex formed in the bcl-2 promoter, the first G-tetrad, also containing three *syn* guanines, was found to be capped by a stable A:T base pair (26). Therefore, the hybrid-type telomeric G-quadruplex in K^+ is likely to be stabilized by the naturally occurring adenine triple capping structure, which appears to be related with the intrinsic asymmetric residue distribution of the tandem TTA loops in the human telomeric DNA sequence.

The hybrid-type G-quadruplex structure appears to be the major conformation formed in the human telomeric sequence in K^+ (23,25). The hybrid-type G-quadruplex conformation, with its 5′- and 3′-ends pointing in opposite directions, can provide an efficient scaffold for the formation of compact-stacking multimer structures in the human telomeric DNA, as discussed in our previous report (23). The basket-type G-quadruplex folding, which

was found to form in a truncated Tel22 (Figure 1A) sequence in Na^+ solution (33), is unlikely to form in the extended telomeric sequence in K^+, presumably due to a combination of the steric interference of the two flanking ends and the cation effect of K^+ (23,24). In the presence of K^+, the basket-type Na^+ telomeric G-quadruplex readily converts to the hybrid-type telomeric G-quadruplex, likely through a strand-reorientation mechanism as suggested in our previous report (23).

The hybrid-type telomeric G-quadruplex contains an unusual 3-nt-sized double-chain-reversal loop adopted by the first TTA segment (Figure 6). Such double-chain-reversal loop conformations have only been observed with short loop sizes of 1- and 2-nt in the previously reported studies (23,28,29,36–38). A loop longer than 2-nt is in general not as favored for the formation of double-chain-reversal loop conformation, likely due to the lack of stacking interactions of loop residues in such a conformation. It is interesting to note that, in our structure, the A9 residue of the first TTA loop participates in the adenine triple platform and is positioned above the top tetrad (Figure 7A), making the first TTA double-chain-reversal loop equivalent to a 2-nt-sized loop. This may explain why a 3-nt double-chain-reversal loop can be stably present in this hybrid-type telomeric G-quadruplex structure. The parallel-stranded G-quadruplex (32), in which all three 3-nt TTA loops are in double-chain-reversal conformation, is thus unlikely to be stable in K^+ solution (23–25). This has also been suggested by a number of previous studies, including UV studies (39,40), a ^{125}I-radioprobing study (41), a platinum cross-linking study (42), a FRET study (43), a chemical ligation study (44) and a more recent biophysical study (34) in which sedimentation coefficients and 2-AP fluorescence were used. Gratifyingly, the calculation of hydrodynamic properties on our structure gave a sedimentation coefficient (S) value of 2.07 with no K^+ ions bound, or an S value of 2.09 with two K^+ ions bound (kindly performed by Prof. John Trent at the University of Louisville). These values are in excellent agreement with the experimentally observed value of 2.11 (1.5% difference) (34). This result also shows that a sedimentation coefficient is a reliable measure for different G-quadruplex structures. Thus an important conclusion made from our determined structure is that it can fully explain the results and predictions made in previous studies where physiologically relevant conditions were used with the wild-type human telomeric sequence.

We have observed a possible A:T base pair (A25:T14) capping the bottom tetrad in our structure (Figure 8B), in which A25 is a mutated residue from the native thymine in the human telomeric sequence (Figure 1A). This may explain our finding that the 3′-flanking adenine helps to stabilize the telomeric G-quadruplex in K^+ (23). A native 23-mer telomeric sequence lacking this mutated adenine (Tel23, Figure 1A) also adopts the hybrid-type G-quadruplex as the major conformation (70%) (25). However, it is important to note that this native Tel23 sequence contains the important 5′-flanking adenine residue (equivalent to the A3 in our structure), which is needed for the formation of the adenine triple capping structure to stabilize the hybrid-type telomeric G-quadruplex structure in K^+.

In summary, the unique human telomeric G-quadruplex structure formed in K^+ suggests that it can be specifically targeted for anticancer drug design. The formation of the novel adenine triple capping structure may provide a specific binding site for drug targeting.

SUPPLEMENTARY DATA

Supplementary Data is available at NAR Online.

ACKNOWLEDGEMENTS

We thank Dr. Laurence Hurley for insightful comments and suggestions. We thank Dr. John Trent at the University of Louisville for performing the HYDROPRO calculations on our structures. We thank Dr. Megan Carver for technical help and proofreading the manuscript. This research was supported by the National Institutes of Health (1K01CA83886 and 1S10 RR16659). The Open Access publication charges were waived by Oxford University Press.

Conflict of interest statement. None declared.

REFERENCES

1. Blackburn,E.H. and Gall,J.G. (1978) A tandemly repeated sequence at the termini of extrachromosomal ribosomal RNA genes in Tetrahymena. *J. Mol. Biol.*, **120**, 33–53.
2. Allshire,R.C., Dempster,M. and Hastie,N.D. (1989) Human telomeres contain at least 3 types of G-rich repeat distributed non-randomly. *Nucleic Acids Res.*, **17**, 4611–4627.
3. de Lange,T., Shine,L., Myers,R.M., Cox,D.R., Naylor,S.L., Killery,A.M. and Varmus,H.E. (1990) Structure and variability of human chromosome ends. *Mol. Cell. Biol.*, **10**, 518–527.
4. Moyzis,R.K., Buckingham,J.M., Cram,L.S., Dani,M., Deaven,L.L., Jones,M.D., Meyne,J., Ratliff,R.L. and Wu,J.R. (1988) A highly conserved repetitive DNA sequence, $(TTAGGG)_n$, present at the telomeres of human chromosomes. *Proc. Natl. Acad. Sci. U.S.A.*, **85**, 6622–6626.
5. Makarov,V.L., Hirose,Y. and Langmore,J.P. (1997) Long G tails at both ends of human chromosomes suggest a C strand degradation mechanism for telomere shortening. *Cell*, **88**, 657–666.
6. Harley,C.B., Futcher,A.B. and Greider,C.W. (1990) Telomeres shorten during ageing of human fibroblasts. *Nature*, **345**, 458–460.
7. Greider,C.W. and Blackburn,E.H. (1985) Identification of a specific telomere terminal transferase activity in Tetrahymena extracts. *Cell*, **43**, 405–413.
8. Kim,N.W., Piatyszek,M.A., Prowse,K.R., Harley,C.B., West,M.D., Ho,P.L., Coviello,G.M., Wright,W.E., Weinrich,S.L. *et al.* (1994) Specific association of human telomerase activity with immortal cells and cancer. *Science*, **266**, 2011–2015.
9. Hanahan,D. and Weinberg,R.A. (2000) The hallmarks of cancer. *Cell*, **100**, 57–70.
10. Mergny,J.L. and Helene,C. (1998) G-quadruplex DNA: a target for drug design. *Nat. Med.*, **4**, 1366–1367.
11. Sun,D.Y. and Hurley,L.H. (2001). Chaires,JB and Waring,MJ (eds), *Methods in Enzymology, drug-nucleic acid interactions* Academic Press, Inc., Vol. 340, pp. 573–592.
12. Hurley,L.H. (2002) DNA and its associated processes as targets for cancer therapy. *Nat. Rev. Cancer*, **2**, 188–200.
13. Neidle,S. and Parkinson,G. (2002) Telomere maintenance as a target for anticancer drug discovery. *Nat. Rev. Drug Discov.*, **1**, 383–393.
14. Bodnar,A.G., Ouellette,M., Frolkis,M., Holt,S.E., Chiu,C.P., Morin,G.B., Harley,C.B., Shay,J.W., Lichtsteiner,S. *et al.* (1998)

Extension of life-span by introduction of telomerase into normal human cells. *Science*, **279**, 349–352.
15. Harley,C.B. (1991) Telomere loss: mitotic clock or genetic time bomb? *Mutat. Res.*, **256**, 271–282.
16. Sun,H., Karow,J.K., Hickson,I.D. and Maizels,N. (1998) The Bloom's syndrome helicase unwinds G4 DNA. *J. Biol. Chem.*, **273**, 27587–27592.
17. Sun,H., Bennett,R.J. and Maizels,N. (1999) The saccharomyces cerevisiae Sgs1 helicase efficiently unwinds G-G paired DNAs. *Nucleic Acids Res.*, **27**, 1978–1984.
18. Hackett,J.A., Feldser,D.M. and Greider,C.W. (2001) Telomere dysfunction increases mutation rate and genomic instability. *Cell*, **106**, 275–286.
19. Salazar,M., Thompson,B.D., Kerwin,S.M. and Hurley,L.H. (1996) Thermally induced DNA:RNA hybrid to G-quadruplex transitions: possible implications for telomere synthesis by telomerase. *Biochemistry*, **35**, 16110–16115.
20. Hurley,L.H. (2001) Secondary DNA structures as molecular targets for cancer therapeutics. *Biochem. Soc. Trans.*, **29**, 692–696.
21. Hurley,L.H., Wheelhouse,R.T., Sun,D., Kerwin,S.M., Salazar,M., Fedoroff,O.Y., Han,F.X., Han,H.Y., Izbicka,E. *et al.* (2000) G-quadruplexes as targets for drug design. *Pharmacol. Ther.*, **85**, 141–158.
22. Neidle,S. and Read,M.A. (2000) G-quadruplexes as therapeutic targets. *Biopolymers*, **56**, 195–208.
23. Ambrus,A., Chen,D., Dai,J.X., Bialis,T., Jones,R.A. and Yang,D.Z. (2006) Human telomeric sequence forms a hybrid-type intramolecular G-quadruplex structure with mixed parallel/antiparallel strands in potassium solution. *Nucleic Acids Res.*, **34**, 2723–2735.
24. Xu,Y., Noguchi,Y. and Sugiyama,H. (2006) The new models of the human telomere d[AGGG(TTAGGG)(3)] in K+ solution. *Bioorg. Med. Chem.*, **14**, 5584–5591.
25. Luu,K.N., Phan,A.T., Kuryavyi,V., Lacroix,L. and Patel,D.J. (2006) Structure of the human telomere in K+ solution: an intramolecular (3+1) G-quadruplex scaffold. *J. Am. Chem. Soc.*, **128**, 9963–9970.
26. Dai,J.X., Chen,D., Jones,R.A., Hurley,L.H. and Yang,D.Z. (2006) NMR solution structure of the major G-quadruplex structure formed in the human BCL2 promoter region. *Nucleic Acids Res.*, **34**, 5133–5144.
27. Dai,J.X., Punchihewa,C., Mistry,P., Ooi,A.T. and Yang,D.Z. (2004) Novel DNA bis-intercalation by MLN944, a potent clinical bisphenazine anticancer drug. *J. Biol. Chem.*, **279**, 46096–46103.
28. Ambrus,A., Chen,D., Dai,J.X., Jones,R.A. and Yang,D.Z. (2005) Solution structure of the biologically relevant G-quadruplex element in the human c-MYC promoter. Implications for G-quadruplex stabilization. *Biochemistry*, **44**, 2048–2058.
29. Dai,J., Dexheimer,T.S., Chen,D., Carver,M., Ambrus,A., Jones,R.A. and Yang,D. (2006) An intramolecular G-quadruplex structure with mixed parallel/antiparallel G-strands formed in the human BCL-2 promoter region in solution. *J. Am. Chem. Soc.*, **128**, 1096–1098.
30. Brünger,A.T. (1993) *X-PLOR Version 3.1: A System for X-ray Crystallography and NMR*. Yale University Press, New Haven, CT, USA.
31. Wijmenga,S.S. and van Buuren,B.N.M. (1998) The use of NMR methods for conformational studies of nucleic acids. *Prog. Nucl. Magn. Reson. Spectrosc.*, **32**, 287–387.
32. Parkinson,G.N., Lee,M.P.H. and Neidle,S. (2002) Crystal structure of parallel quadruplexes from human telomeric DNA. *Nature*, **417**, 876–880.
33. Wang,Y. and Patel,D.J. (1993) Solution structure of the human telomeric repeat d[AG(3)(T(2)AG(3))3] G-tetraplex. *Structure*, **1**, 263–282.
34. Li,J., Correia,J.J., Wang,L., Trent,J.O. and Chaires,J.B. (2005) Not so crystal clear: the structure of the human telomere G-quadruplex in solution differs from that present in a crystal. *Nucleic Acids Res.*, **33**, 4649–4659.
35. Nicholls,A., Sharp,K.A. and Honig,B. (1991) Protein folding and association–insights from the interfacial and thermodynamic properties of hydrocarbons. *Proteins Struct. Funct. Genet.*, **11**, 281–296.
36. Seenisamy,J., Rezler,E.M., Powell,T.J., Tye,D., Gokhale,V., Joshi,C.S., Siddiqui-Jain,A. and Hurley,L.H. (2004) The dynamic character of the G-quadruplex element in the c-MYC promoter and modification by TMPyP4. *J. Am. Chem. Soc.*, **126**, 8702–8709.
37. Phan,A.T., Modi,Y.S. and Patel,D.J. (2004) Propeller-type parallel-stranded G-quadruplexes in the human c-myc promoter. *J. Am. Chem. Soc.*, **126**, 8710–8716.
38. Sun,D.Y., Guo,K.X., Rusche,J.J. and Hurley,L.H. (2005) Facilitation of a structural transition in the polypurine/polypyrimidine tract within the proximal promoter region of the human VEGF gene by the presence of potassium and G-quadruplex-interactive agents. *Nucleic Acids Res.*, **33**, 6070–6080.
39. Balagurumoorthy,P. and Brahmachari,S.K. (1994) Structure and stability of human telomeric sequence. *J. Biol. Chem.*, **269**, 21858–21869.
40. Rezler,E.M., Seenisamy,J., Bashyam,S., Kim,M.Y., White,E., Wilson,W.D. and Hurley,L.H. (2005) Telomestatin and diseleno sapphyrin bind selectively to two different forms of the human telomeric G-quadruplex structure. *J. Am. Chem. Soc.*, **127**, 9439–9447.
41. He,Y.J., Neumann,R.D. and Panyutin,I.G. (2004) Intramolecular quadruplex conformation of human telomeric DNA assessed with I-125-radioprobing. *Nucleic Acids Res.*, **32**, 5359–5367.
42. Redon,S., Bombard,S., Elizondo-Riojas,M.A. and Chottard,J.C. (2003) Platinum cross-linking of adenines and guanines on the quadruplex structures of the AG(3)(T(2)AG(3))(3) and (T(2)AG(3))(4) human telomere sequences in Na+ and K+ solutions. *Nucleic Acids Res.*, **31**, 1605–1613.
43. Ying,L.M., Green,J.J., Li,H.T., Klenerman,D. and Balasubramanian,S. (2003) Studies on the structure and dynamics of the human telomeric G quadruplex by single-molecule fluorescence resonance energy transfer. *Proc. Natl. Acad. Sci. U.S.A.*, **100**, 14629–14634.
44. Qi,J.Y. and Shafer,R.H. (2005) Covalent ligation studies on the human telomere quadruplex. *Nucleic Acids Res.*, **33**, 3185–3192.